# Temporal Variations in Atmospheric Water Vapor and Aerosol Optical Depth Determined by Remote Sensing

DAVID E. PITTS, W. E. MCALLUM, MICHAEL HEIDT AND KEITH JESKE

*Lyndon B. Johnson Space Center, NASA, Houston, Tex. 77058*

J. T. LEE

*National Severe Storm Laboratory, NOAA, Norman, Okla. 73069*

DAN DEMONBRUN, AL MORGAN AND JOHN POTTER

*Lockheed Electronics Company, Houston, Tex. 77058*

(Manuscript received 9 August 1976, in revised form 12 September 1977)

ABSTRACT

By automatically tracking the sun, a four-channel solar radiometer was used to continuously measure optical depth and atmospheric water vapor. The design of this autotracking solar radiometer is presented to allow construction by the reader. A technique for calculating the precipitable water from the ratio of a water band to a nearby nonabsorbing band is discussed. Studies of the temporal variability of precipitable water and atmospheric optical depth at 0.610, 0.8730 and 1.04 $\mu$m are presented. There was good correlation between the optical depth measured using the autotracker and visibility determined from nearby National Weather Service Station data. However, much more temporal structure was evident in the autotracker data than in the visibility data. Cirrus clouds caused large changes in optical depth over short time periods. They appear to be the largest deleterious atmospheric effect over agricultural areas that are remote from urban pollution sources. Cirrus clouds also caused anomalously low estimates of precipitable water.

## 1. Introduction

As viewed by instruments on satellites, absorption by atmospheric water vapor and scattering by atmospheric aerosols change the spectral signatures of ground scenes. When the energy transmitted through the atmosphere is much greater than the thermal emission by the atmosphere, the effect of an absorbing gas is to decrease the reflected solar intensity by a multiplicative factor. The effect of atmospheric aerosols is to decrease the intensity by a multiplicative factor and to increase the intensity by an additive factor. If horizontal gradients of optical depth exist, horizontal gradients will be superimposed on the background scene. Using automatic pattern recognition techniques, digital data analysis compensates for these effects if the training and unknown areas are sensed under the same circumstances. If, however, a class signature is used to classify an area separated either by time or distance, then the probability increases that the atmosphere will cause perturbations on the scene and this will decrease the accuracy of the classification (Turner, 1975).

At the present time little is known about the variability of the atmosphere on the scale of 1:100 km and 1:100 min. The purpose of this experiment was to determine small-scale and short-term changes in optical depth of test cases and to determine the importance of developing satellite systems to expand objective aerosol measurements to a global scale. Because of the global aspect of the satellite programs, ground-based radiometers would not be practical to support an operational system. However, small networks of automatic radiometers can be used to define the variability of environments (e.g., near severe thunderstorms) before establishing remote sensing techniques to measure these parameters from space.

Solar radiometry is a widely established technique, which has been used to measure background atmospheric turbidity (Flowers *et al.*, 1969; Volz, 1969). This technique has been used to measure aerosol and gaseous pollution and to indicate the genesis of large volcanic eruptions (Volz, 1975). Likewise, Wilkins and Suggs (personal communication) have shown that horizontal moisture gradients and incipient clouds that are invisible to the naked eye can be found by this technique. These clouds can cause significant variability in the transmission of energy through the atmosphere.

To determine total atmospheric precipitable water, Fowle (1912, 1915) first established the method of using band ratios of a water absorption line to a nearby window in the near infrared. Gates (1956) refined and

calibrated the technique for the 0.94, 1.13 and 1.38 $\mu$m water vapor bands. Later, Gates and Harrop (1963) found that the natural logarithm of the ratio between the center of a water vapor band and a nonabsorbing band was linearly related to the square root of precipitable water. Guzzi *et al.* (1972) used the 1.13 $\mu$m band to calculate precipitable water and found that cirrus clouds caused large errors in these calculations. During a two-year period in Norway, Sivertsen and Solheim (1975a,b) used a polarizing radiometer covering the 1.91 $\mu$m water vapor band and found that precipitable water is usually at a maximum near noon. Volz (1974) described a multispectral sun photometer that could determine atmospheric precipitable water by using the ratio of the 0.94 $\mu$m water vapor band to the 0.88 $\mu$m nonabsorbing band and square root law of band absorption.

In an independent investigation, the authors derived a functional relationship between water vapor transmission and clear band transmission. This was done by using the predictions resulting from "Atmospheric Transmission Computer Program CP" (Pitts *et al.*, 1974a,b). This corroborated the model of Gates and Harrop (1963). However, for the particular filters used to cover the 0.94 $\mu$m water vapor band and the 0.87 $\mu$m nonabsorbing band, the exponent of the precipitable water was 1/1.78 instead of $\frac{1}{2}$ which Volz and Gates and Harrop used.

## 2. Autotracking solar radiometer design

A seven-channel photometer (Fig. 1) was designed at the Lyndon B. Johnson Space Center to determine the atmospheric effects on Landsat multispectral scanner data. This unit is similar to the Volz two-channel unit that uses the 0.38 and 0.50 $\mu$m channels but utilizes the 0.38, 0.50, 0.61, 0.75, 0.87 and 1.04 $\mu$m channels for measuring optical depth and the 0.942 $\mu$m channel for precipitable water. Since 1972, approximately 30 of these units have been constructed and used at various agricultural locations in the Great Plains, the corn belt and the Pacific Northwest. In training observers to use these instruments, several significant problems arose:

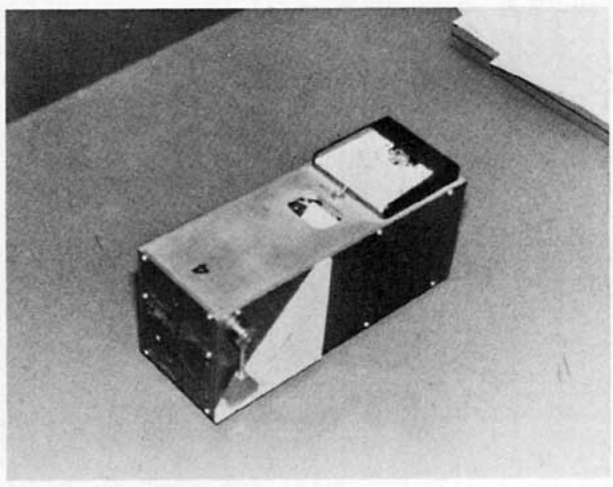

FIG. 1. Seven-channel solar radiometer.

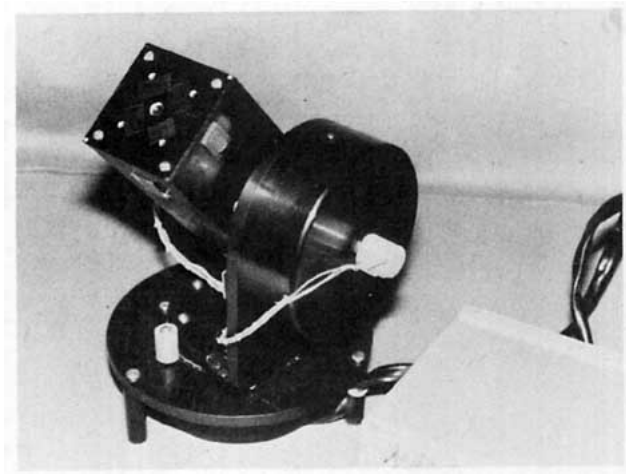

FIG. 2. Autotracking solar radiometer.

1) Measurements on a time scale of minutes are difficult and tiring for one observer to handle.

2) Measurements on a time scale of minutes are needed near satellite passage to determine some environments adequately.

3) Without multiple observations, errors of meter reading and data recording can occur and remain unnoticed.

DeMonbrun's autotracking radiometer system (Fig. 2) consists of four boresighted radiometers, each having a 2° field of view. Interference filters 0.01 $\mu$m wide at the half-power point centered at 0.61, 0.873, 0.942 and 1.04 $\mu$m are used to selectively limit incident solar intensity on the four silicon detectors. Because each band is sensed by a dedicated radiometer, the sampling rate of the system is determined by the sampling rate of the digital recorder. The unit incorporates an alt-azimuth mount with a servomotor on both axes, each responding to two external sun sensors for coarse alignment located on the instrument sides and to two internal sun sensors for fine alignment. The electronics and configuration of the radiometer are shown on Fig. 3. The alt-azimuth mount with servomechanism was chosen instead of an equatorial drive (Shaw *et al.*, 1973) to reduce setup and alignment procedures and to enable the observer to use the instrument on mobile platforms. The prototype unit was constructed using off-the-shelf supplies at a cost of approximately $2000, but units can be constructed for as little as $1000.

## 3. Data reduction and calibration

Cassette tapes produced in the field by the Metrodata digital recorder are processed on a Nova 1200 mini-

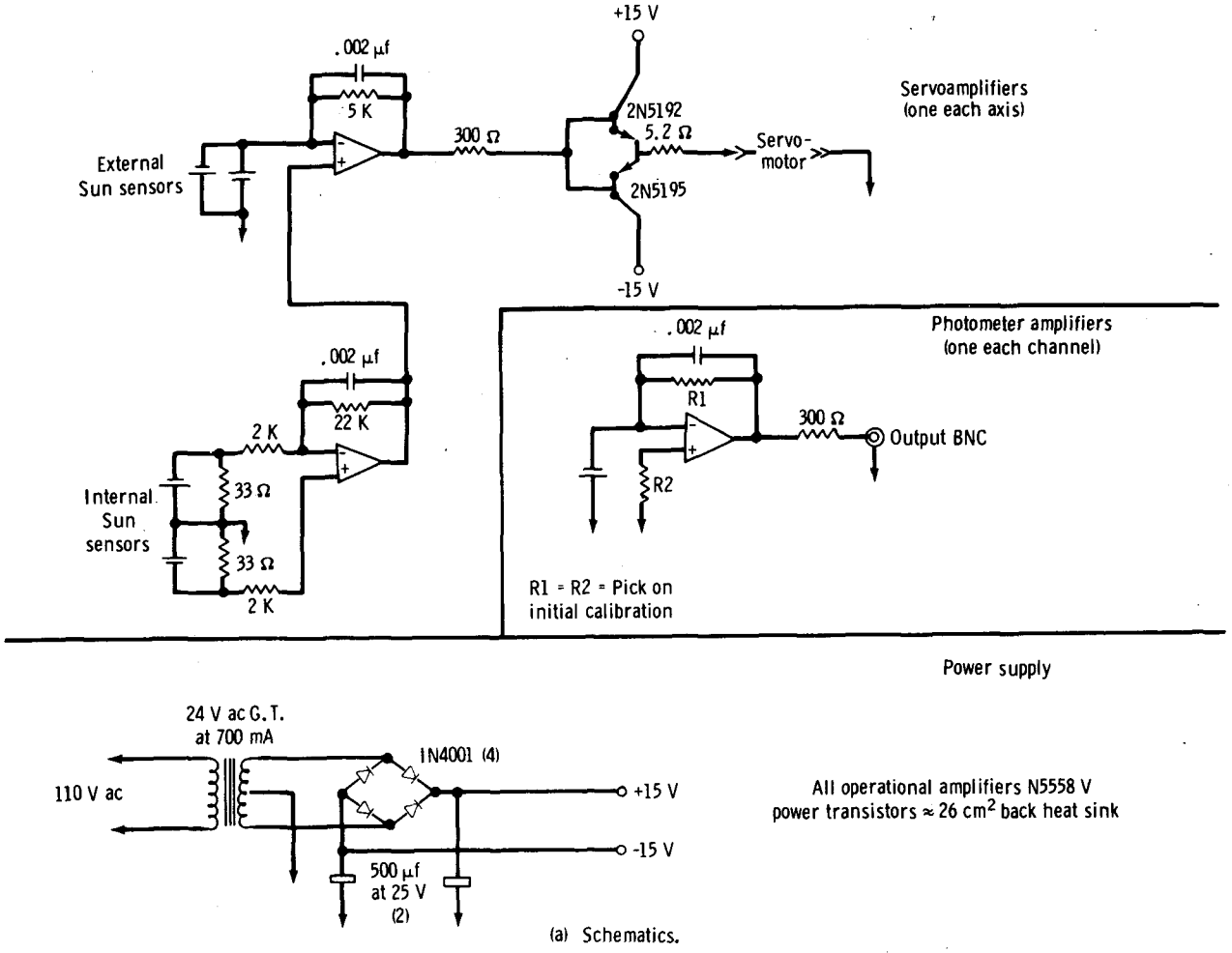


(a) Schematics.

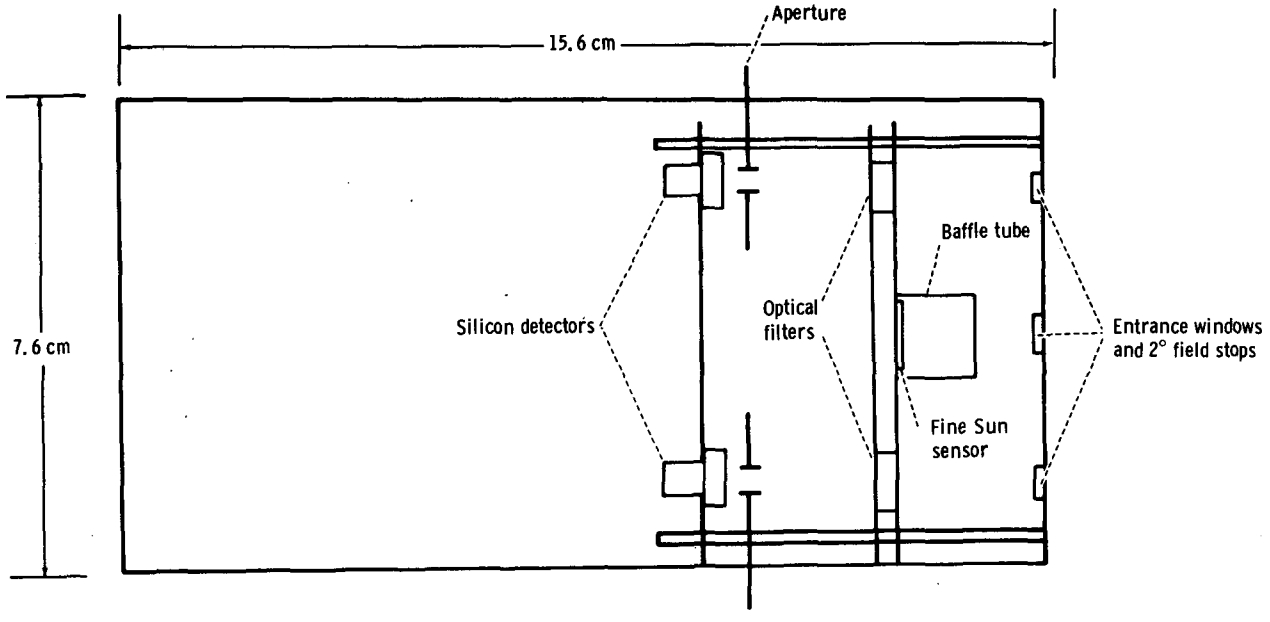


(b) Configuration.

FIG. 3. Solar radiometer details.

computer system to edit bad scans and reformat the data onto a nine-track computer-compatible tape. Final data reduction is handled by FORTRAN software on the Univac 1108 computer. Scans are averaged and standard deviations are calculated over 1 min periods. Means, standard deviations and other statistical comparisons are calculated for each day and channel. Precipitable water in the slant path from the radiometer to the sun was calculated from the empirically derived equation of Pitts *et al.*, (1974a), i.e.,

$$W=\frac{p\cos\theta}{0.218p_0}\left(\ln\frac{1}{\bar{T}}\right)^{1.78}, \tag{1}$$

where $W$ is precipitable water (cm), $p$ the surface pressure (mb), $\theta$ the solar zenith angle, $p_0=1013.25$ mb, $\bar{T}=C(J_{0.9420}/J_{0.8730})$, and $C=0.584$.

The constant $C$ is evaluated during the calibration period by comparing radiometer data with precipitable water determined from nearby radiosonde measurements. Included in this constant are the relative gains in the two channels. Because the 0.9420 $\mu$m water band obeys the square root law and not the Beers law, $C$ is not the ratio of the $J_0$ readings of the two channels obtained by a Rayleigh calibration.

The factor $\cos\theta$ converts the precipitable water measurement from a slant path to a vertical path. To calculate this factor, the hour angle $H$ was calculated from the time stored on the digital recording tape with each set of four radiometer readings. $\cos\theta$ was then calculated from

$$\cos\theta=\sin\phi\sin\delta+\cos\phi\cos\delta\cos H, \tag{2}$$

where $\theta$ is solar zenith angle, $\phi$ the latitude of the autotracker, $\delta$ the solar declination and

$$H=(\mathrm{GMT}-12)15-L,$$

where GMT is Greenwich mean time (hours) and $L$ the longitude (deg) of the autotracker.

Atmospheric optical depth $\tau_i$ for the aerosol channels was calculated from the output voltage $J_i$ using the Beer law (Shaw *et al.*, 1973)

$$\tau_i=-\cos\theta\ln(J_i/J_{0i}). \tag{3}$$

The calibration voltage at zero airmass $J_{0i}$ was determined by the Rayleigh calibration method.

In addition to the Rayleigh calibration, a relative calibration method can be used which is not constrained by the requirement of having the optical depth at a constant level throughout the entire day. This requires that one precalibrated solar radiometer be used as a standard unit to calibrate another unit by simultaneously recording voltage outputs for the same channel for both units and averaging for several minutes. Then Eq. (3) can be solved for the calibration value of the other radiometer $J_0'$ in terms of its average voltage $\overline{J'}$, the calibration value of the standard unit $J_0$, and the average voltage in the standard unit $\bar{J}$:

$$J_0'=(\overline{J'}/\bar{J})J_0. \tag{4}$$

Experience at the Johnson Space Center in calibrating solar radiometers in non-water-absorption bands by the ratio method indicates coefficients of variation as large as 13% for the ratio of calibration values between two simultaneous measurements. The average precision for seven bands from 0.38 to 1.04 $\mu$m is between 3 and 6%. The results of many days of gathering data at approximately 100 measurements per minute indicate that the autotracker unit allows precision of 0.1–1.0% over a 1 min period. Thus, digital recording with its associated larger number of measurements and dynamic range offers additional precision when used with the ratio method of calibration.

### *a. Tracking accuracy*

To test the accuracy of the autotracking system, the base of the autotracker was manually tilted and rotated through increments of approximately 45° in azimuth while sampling the radiometers at 33 samples per minute. Before the base was moved to perturb the autotracking system, the coefficient of variation due to the atmosphere was about 0.3% (142 samples) for each of the channels. The interval from the beginning of the perturbation to the time of recovery (within 2% of the steady-state value) was 3–5 s. This test was much more rigorous than the conditions that would occur in the field or on a mobile platform because the changes were rapid and large angles were involved. However, because recovery time is so short, errors caused by poor tracking can be eliminated by running mean comparisons over 5–10 s. Doing this will still allow a 100 m resolution of optical depth structure while traveling on a mobile platform at highway speeds.

### *b. Errors as a function of time of day*

To understand the error in optical depth caused by an error in the calibration voltage $J_{0i}$, one may calculate the partial derivative of Eq. (3) with respect to $\ln J_{0i}$. The sensitivity of the water vapor estimator can be determined by taking the partial derivative of Eq. (1) with respect to $\ln C$. Both functions are proportional to $\cos\theta$, which indicates that an error in calibration effects the estimate more at local solar noon.

### *c. Errors due to diffuse scattering in the atmosphere*

Shaw *et al.* (1973) have calculated that diffuse scattering into the field of view of the radiometer is less than 2% of the direct intensity when the optical depth is less than 0.5. However, when optical depths exceed 0.5, multiple scattering into the forward direction increases the intensity received by the radiometer and causes underestimations in optical depth. To calculate

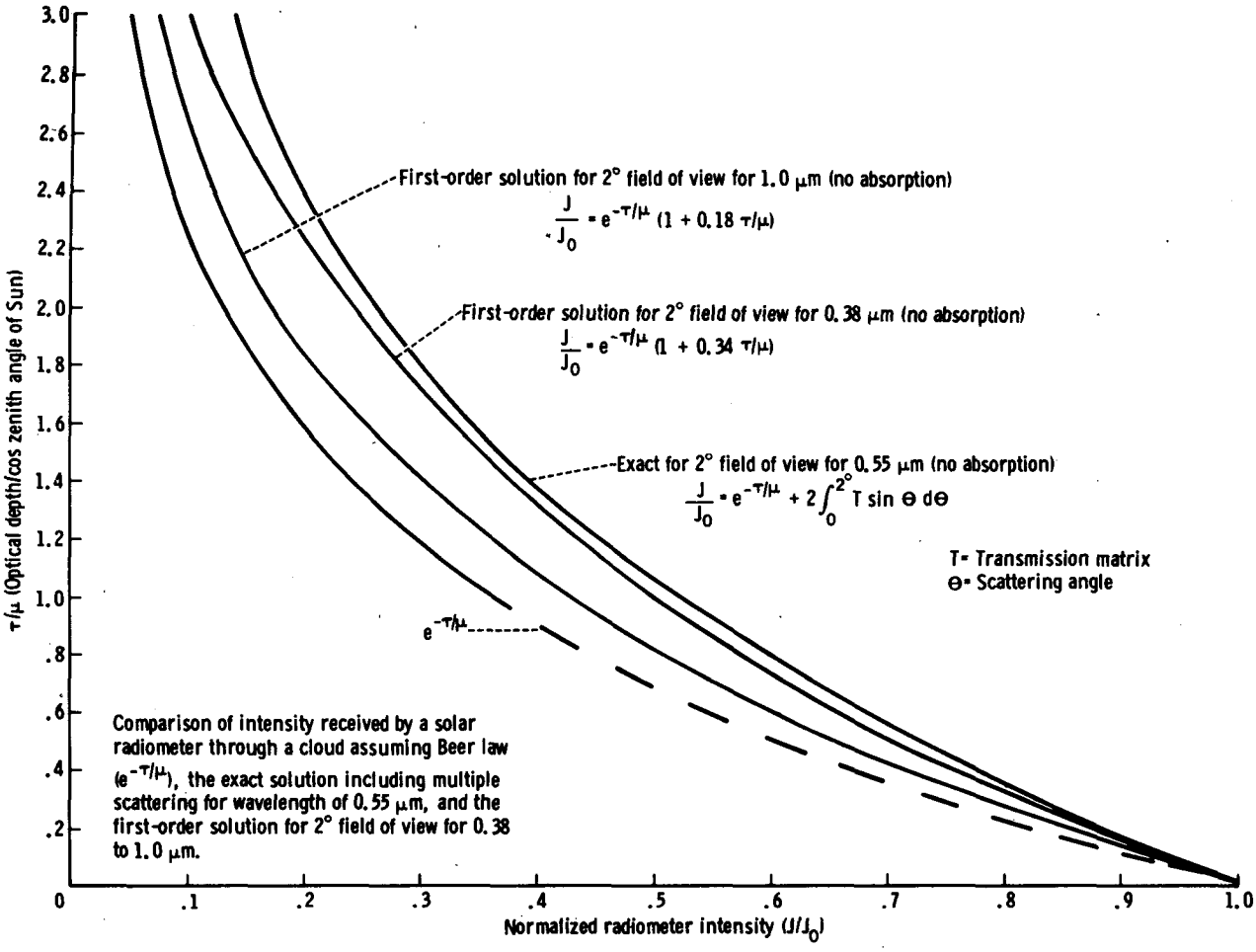


FIG. 4. Optical depth vs normalized radiometer output for the Deirmendjian (1964) C1 cloud model.

how these errors affect the results when single scattering is assumed, the C1 cloud model of Deirmendjian (1964) was used for two cases: 1) exact (effects of the multiple scattering were calculated for all orders of multiple scattering) and 2) first order. Computational methods that incorporate the doubling method of Hansen (1969, 1971) were used to solve the radiative-transfer equations. The data in Fig. 4 indicate that, for a given incident intensity at the radiometer, a Beer law extinction [Eq. (3)] underestimates the optical depth of clouds as compared to first-order or exact solutions. This underestimation is primarily due to the forward scattering increasing the intensity toward the radiometer as compared to isotropic scattering. At optical depths of 1.2, the Beer law underestimates the cloud optical depth by 40%. The first-order solution, however, corrects most of this error and can easily be solved for $\tau$ by iterative techniques such as Newton's method.

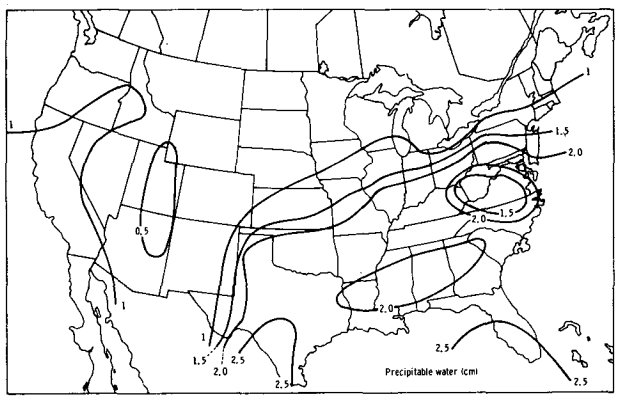


FIG. 5. Precipitable water chart for 0000 GMT 8 March 1974.

## 4. Case studies

### *a. 7 March 1974 case, Houston, Texas*

Data were collected at the Johnson Space Center on 7 March 1974 from 1520 to 1840 (all times GMT). The precipitable water chart for the United States for 0000 on 8 March 1974 is shown on Fig. 5. No large horizontal gradients were evident in east Texas on the scale of the radiosonde launching stations (400 km). The surface reports for Ellington Air Force Base, which is several kilometers northwest of the Johnson Space

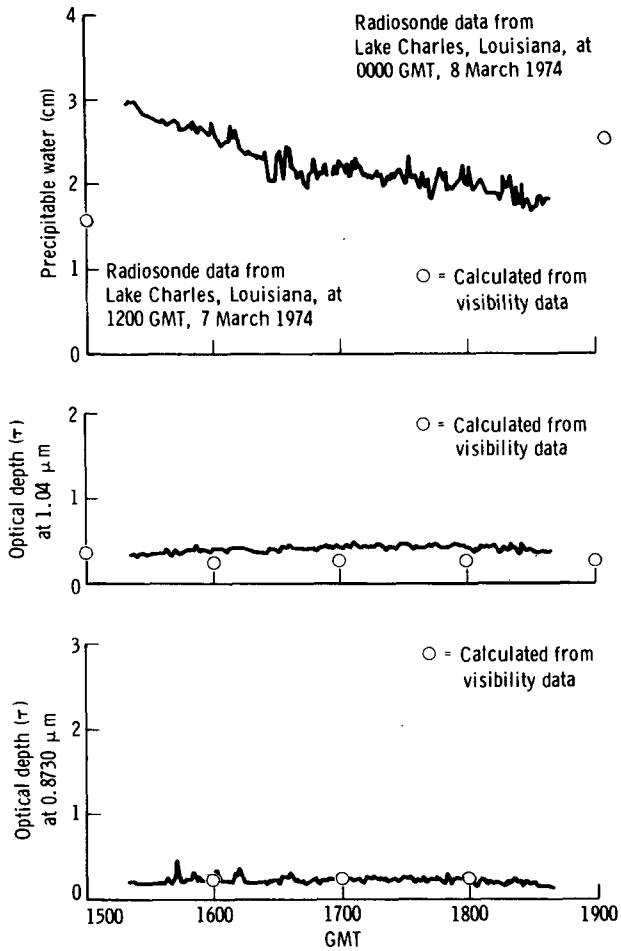


FIG. 6. Precipitable water and optical depth of the atmosphere at the Johnson Space Center for 7 March 1974.

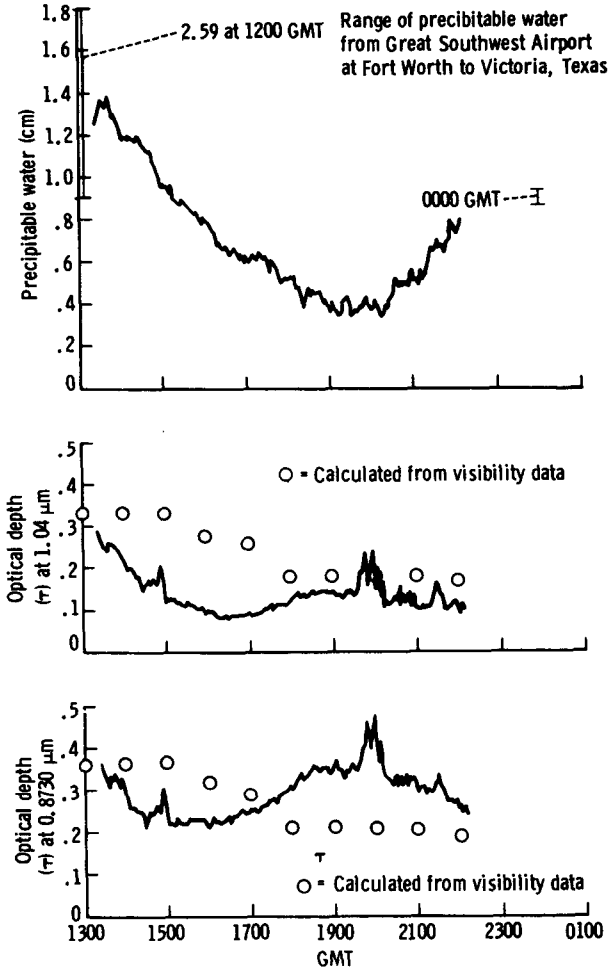


FIG. 7. Precipitable water and optical depth of the atmosphere at Austin, Tex., for 3 April 1974.

Center, indicated low-altitude cumulus (0.4 km, scattered) and high-altitude cirrus (9.1 km, scattered); the surface dewpoint-temperature difference ranged between 6 and 9 K, wind speeds ranged from 7 to 11 m $s^{-1}$ and the visibility was constant at 24 km.

The autotracker-measured precipitable water (Fig. 6) decreased from 3.0 to 1.75 cm for the period from 1530 to 1840. The radiosondes at Lake Charles, La., increased from 1.6 cm at 1200 GMT to 2.25 cm at 0000 GMT. However, the dewpoint-temperature difference at Ellington Air Force Base increased during the day, which confirmed the decrease in precipitable water measured by the autotracker.

The visibility data from the hourly surface observations were converted to optical depth $\tau$ using the formula of Elterman (1970).

Excellent agreement between the surface visibility and the optical depth as a function of time for 1.04 and 0.8730 $\mu$m is shown on Fig. 6. The 0.61 $\mu$m channel was inoperative this day.

### *b. 3 April 1974 case, Austin, Texas*

This case shows a dramatic decrease from 1.3 cm at 1330 GMT to 0.4 cm at 2000 GMT as a dry front passed over central Texas (Fig. 7). Some high-altitude cirrus was evident throughout the day. Figs. 8 and 9

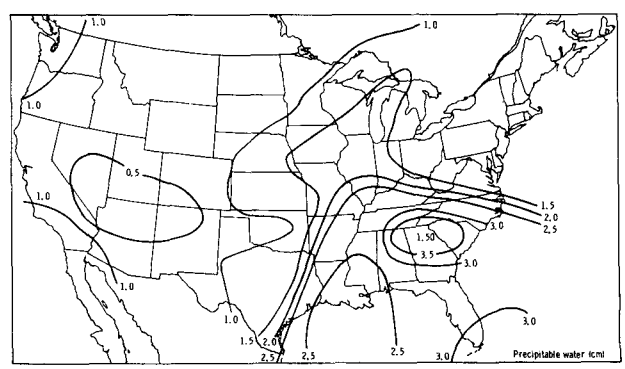


FIG. 8. Precipitable water chart for 1200 GMT 3 April 1974.

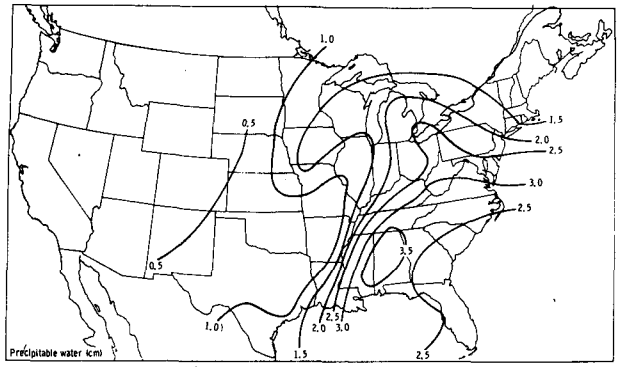


FIG. 9. Precipitable water chart for 0000 GMT 4 April 1974.

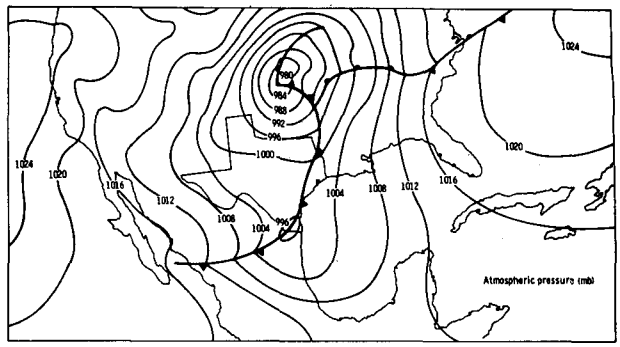


FIG. 10. Surface chart for 1500 GMT 3 April 1974.

show the precipitable water charts for 1200 on 3 April and 0000 on 4 April, respectively. Fig. 10 is the surface chart for 1500 on 3 April 1974. The morning radiosonde measurements of precipitable water at Victoria, Tex., and at Great Southwest Airport at Fort Worth, Tex., bracket the autotracker measurement made at 1330. Radiosonde data at 0000 agree closely with the autotracker data taken at 2200. Surface observations at Austin show dust from 1300 to 1900 and a decrease in autotracker optical depth after that time. The autotracker optical depths on Fig. 7 show good agreement but are phase-shifted relative to the calculated optical depths based on the surface observations. The coefficient of variation generally was less than 1% for all aerosol and precipitable water channels. However, the coefficient of variation read 17% for one period in the morning. Between 1930 and 2000 GMT, the optical depths in all three channels (1.04, 0.8730 and 0.9420 $\mu$m) increased.

Because dust was dissipating and some cirrus was evident, it is suspected that cirrus was the cause of the increase. Interestingly, this increased optical depth did not affect the measurement of precipitable water based on the ratio of the 0.9420 and 0.8730 $\mu$m channels. During this period, the coefficient of variation for the 1.04 and 0.8730 $\mu$m channels increased from less than 1% to more than 18%. Precipitable water coefficient of variation increased from 1 to 4%. The 0.61 $\mu$m channel was inoperative for this case.

### *c. 31 March 1975 case, Norman, Oklahoma*

The statistics for twelve 1 min/periods for this case are provided in Table 1. Plots of optical depth and precipitable water for the day are shown on Fig. 11.

TABLE 1. Selected observations of precipitable water ($P$), optical depth ($\tau$) and standard deviation ($S$) at Norman, Okla., for 31 March 1975.

| GMT | Observations (no.) | Precipitable water | | Optical depth for channel i, at - | | | | | |
|---|---|---|---|---|---|---|---|---|---|
| | | P | S | 1.04 μm | | 0.8730 μm | | 0.61 μm | |
| | | (cm) | (cm) | τ | S | τ | S | τ | S |
| 1336 | 113 | 1.0085 | 0.04890 | 0.08298 | 0.00100 | 0.06835 | 0.00556 | 0.08998 | 0.00104 |
| 1337 | 27 | 0.9042 | 0.03150 | 0.08622 | 0.00123 | 0.07975 | 0.00207 | 0.09220 | 0.00087 |
| 1429 | 40 | 0.92496 | 0.00280 | 0.14028 | 0.00078 | 0.06963 | 0.00048 | 0.09000 | 0.00103 |
| 1430 | 65 | 0.92746 | 0.00306 | 0.1430 | 0.00059 | 0.06968 | 0.00054 | 0.08920 | 0.00126 |
| 1534 | 69 | 0.97725 | 0.00496 | 0.15605 | 0.00067 | 0.06075 | 0.00075 | 0.13219 | 0.00253 |
| 1658 | 85 | 0.17885 | 0.00612 | 0.50612 | 0.00551 | 0.63324 | 0.00868 | 0.65107 | 0.00783 |
| 1908 | 120 | 0.90534 | 0.00637 | 0.15314 | 0.00233 | 0.07091 | 0.00129 | 0.28416 | 0.00435 |
| 1943 | 72 | 0.93097 | 0.00709 | 0.15716 | 0.00085 | 0.06458 | 0.00099 | 0.24573 | 0.00371 |
| 2028 | 31 | 0.90588 | 0.00636 | 0.14067 | 0.00091 | 0.07613 | 0.00220 | 0.25388 | 0.00488 |
| 2029 | 55 | 0.92359 | 0.00503 | 0.14256 | 0.00101 | 0.07017 | 0.00107 | 0.23844 | 0.00319 |
| 2130 | 38 | 0.85350 | 0.00339 | 0.09820 | 0.0015 | 0.02959 | 0.00153 | 0.13860 | 0.00235 |
| 2131 | 88 | 0.86454 | 0.00817 | 0.09560 | 0.00124 | 0.02285 | 0.00209 | 0.12892 | 0.00454 |
| Total (or average) for day | 877 | 0.953 | 0.514 | 0.20096 | 0.21510 | 0.16620 | 0.30813 | 0.25985 | 0.28038 |

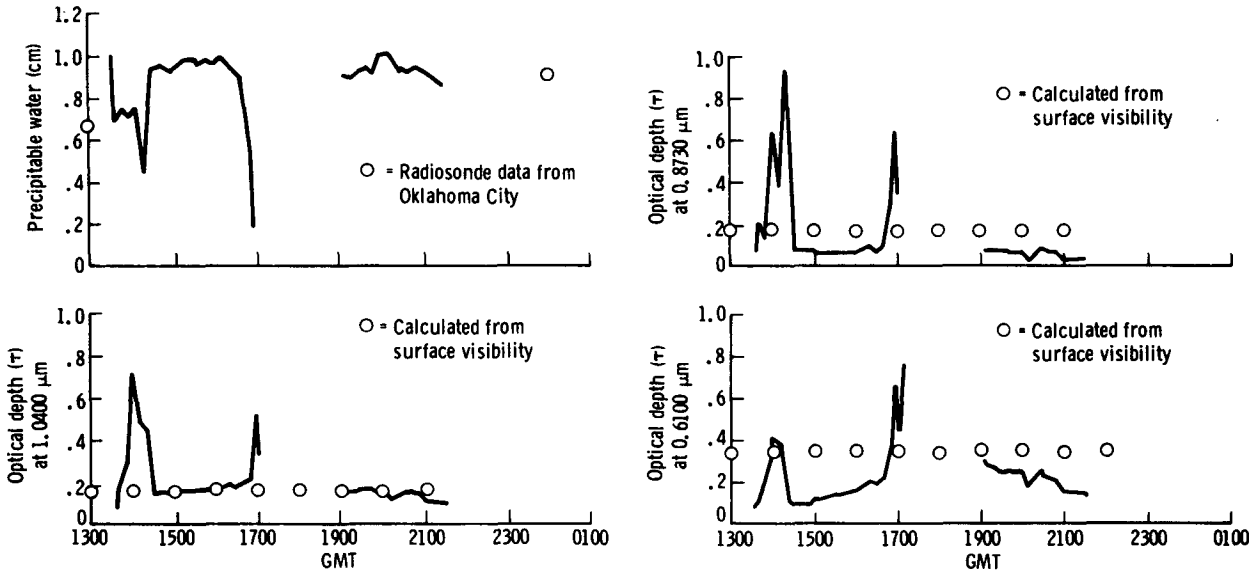


FIG. 11. Precipitable water and optical depth of the atmosphere at Norman, Okla., for 31 March 1975.

The day started clear and scattered cirrus became evident at 1534 GMT and at 1700 the autotracker developed a malfunction. After repair at 1908, a thin uniform cirrus veil with 3/10 sky cover with heavier streaking was evident. During this period, the variance ($S^2$) of all channels increased but the coefficients of variation ($S/\tau$) were still below 1%.

Shortly thereafter, the sky cleared and the optical depths decreased again. The 1.04 $\mu$m channel optical depth was about the same as the morning value, whereas the 0.8730 $\mu$m channel optical depth was less than, and the 0.61 $\mu$m channel optical depth was higher than, the morning value. The precipitable water from the radiometer was about the same all day except from 1330 to 1430 when high variability was evident.

The increased optical depth at 1658 was due to thick cirrus. The duration of the cirrus from 1658 to 1943 and the wind speed from about 245° at approximately 48 m s$^{-1}$ at the tropopause were used to determine that the size of the cirrus patch was about 11 km. It has been observed for this and several other cases that $\tau_{0.8730} > \tau_{1.04}$ when cirrus occurs. Classical models of optical depth due to aerosol scattering (Elterman, 1970) show decreasing optical depth with increasing wavelength. In these test cases, the optical depth of the background at 0.8730 $\mu$m was slightly lower than that at 0.61 or 1.04 $\mu$m. This was due either to an unexpected phenomenon or an error in calibration. During cirrus events, the optical depth at 0.61 and 0.8730 $\mu$m increases by a factor of 10 and optical depth at 1.04 $\mu$m

TABLE 2. As in Table 1 except for 1 April 1975.

| GMT | Observations (no.) | Precipitable water | | Optical depth for channel i, at - | | | | | |
|---|---|---|---|---|---|---|---|---|---|
| | | P | S | 1.04 μm | | 0.8730 μm | | 0.61 μm | |
| | | (cm) | (cm) | τ | S | τ | S | τ | S |
| 1412 | 31 | 1.07296 | 0.00341 | 0.12804 | 0.00242 | 0.07113 | 0.00111 | 0.15818 | 0.00171 |
| 1438 | 59 | 1.03438 | 0.00944 | 0.12666 | 0.00077 | 0.06963 | 0.00109 | 0.13674 | 0.00187 |
| 1637 | 45 | 0.98616 | 0.00469 | 0.14767 | 0.00076 | 0.08533 | 0.0016 | 0.29432 | 0.00263 |
| 1638 | 56 | 0.98436 | 0.00709 | 0.14903 | 0.00091 | 0.08419 | 0.00092 | 0.29333 | 0.00216 |
| 1805 | 73 | 0.87971 | 0.00921 | 0.13608 | 0.0009 | 0.07875 | 0.00196 | 0.39213 | 0.00489 |
| 1953 | 47 | 1.16574 | 0.00545 | 0.12883 | 0.00065 | 0.06843 | 0.00071 | 0.39217 | 0.00359 |
| 1954 | 96 | 1.16346 | 0.00508 | 0.12932 | 0.00096 | 0.06798 | 0.00087 | 0.39028 | 0.00406 |
| 2127 | 99 | 1.77328 | 0.00847 | 0.10113 | 0.00414 | 0.0470 | 0.00384 | 0.25296 | 0.00371 |
| Total (or average) for day | 703 | 1.1398 | 0.35156 | 0.14120 | 0.08413 | 0.0756 | 0.09330 | 0.27986 | 0.12632 |

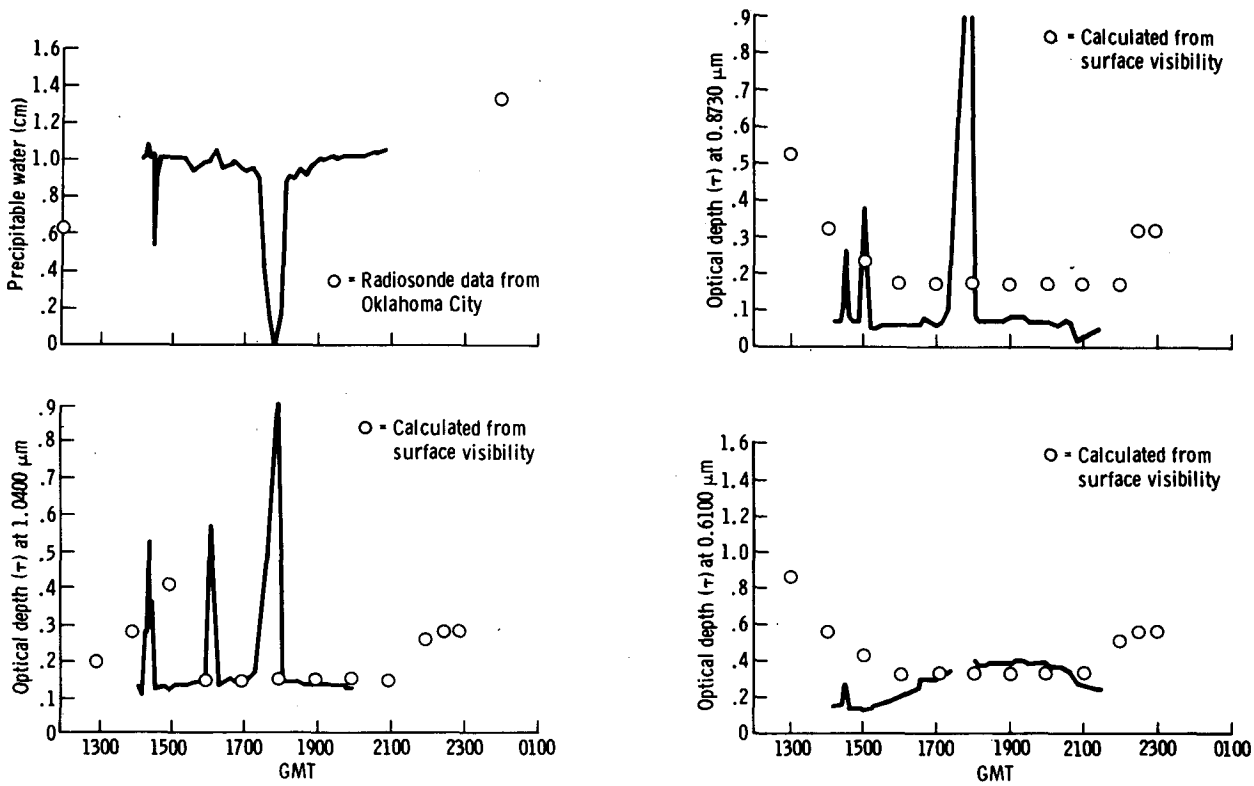


FIG. 12. Precipitable water and optical depth of the atmosphere at Norman, Okla., for 1 April 1975.

increases by a factor of 3. This observation can be used in the data analysis algorithm to prevent cirrus from affecting the precipitable water algorithm.

The radiosonde data for this day showed 0.66 cm at 1200 GMT and 0.90 cm at 0000. The autotracker data showed 1.01 cm at 1336 and 0.86 cm at 2131 (Fig. 11).

*d. 1 April 1975 case, Norman, Oklahoma*

For this case, the statistics for eight 1 min periods are provided in Table 2. Plots of the optical depths and precipitable water from morning to early afternoon are shown on Fig. 12. The day was clear except for the period from 1953 to 2127 when cumulus clouds became evident. The precipitable water decreased from morning until 1805 and then increased to 1.77 cm (Table 2) at the time of cumulus formation. The radiosonde data at 1200 indicated 0.65 cm and those at 0000 indicated 1.34 cm, as compared with the autotracker data of 1.07 cm at 1412 and 1.77 cm at 2127. The optical depth at 1.04 and 0.8730 $\mu$m was almost constant until cumulus formation. The 0.61 $\mu$m channel optical depth and variance was maximum at 1805.

## 5. Conclusions

Temporal studies discussed in this paper indicate that large changes of atmospheric variability can occur over periods ranging from 1 min to several hours. Duggin (personal communication) has determined that the variations in solar irradiance across a Landsat scene are 1–8%. The result of the cases discussed in this paper corroborate Duggin's result showing 1–4% on a scale of 1 min, 20–50% on a scale of 1 h, and 50–100% on a scale of 8 h. Tests of the correlation of optical depth and standard deviation of optical depth, grouped by 1 min intervals, indicate correlation coefficients of 0.80. The probability of this occurring by chance was determined to be 0.002. However, a similar correlation for precipitable water yielded $r=0.2$ and a probability of 0.50, which indicates that this correlation was very likely due to chance. Based on these results, high variability due to cirrus clouds of optical depth over part of a Landsat scene is more likely to occur on days with high optical depth. This is important because future satellite optical depth sensors need only to find high optical depth in one part of a scene to indicate that there will be difficulty analyzing the variable signal from the remainder of the scene. If low optical depths are found, however, the instrument must continue to sample.

In addition, the case studies presented here indicate the following:

1) There is good correlation of optical depth with visibility from a nearby National Weather Service station. Because of higher precision and sampling rates of the radiometers, much more temporal structure was evident in the optical depth data. Furthermore, the

solar radiometer senses cloud contributions to the optical depth, whereas National Weather Service visibility senses horizontal atmospheric conditions.

2) There is good agreement, but at much higher temporal resolution, with radiosonde data for prediction of precipitable water.

3) Cirrus has the property of causing optical depth at 0.8730 $\mu$m to be greater than at 1.04 $\mu$m, permitting cirrus effect removal from the data set used by the percipitable water algorithm.

4) Aerosol effects can be effectively removed from influencing precipitable water estimated by the ratio algorithm. However, cirrus causes anomalously low readings of precipitable water if removal of the effects is not accomplished.

5) Large variations in water vapor of 3 to 1.75 cm occurred during a 3 h period while little variability in aerosol optical depth occurred. This corresponds to a scale of 100 km.

6) Precipitable water decreased from 1.3 to 0.4 cm during a 5 h period during a frontal passage. Large optical depth changes accompanied the precipitable water change. This corresponds to a horizontal scale of 100 km.

7) Coefficients of variation of optical depth of 20–50% were measured over periods of 30 min to several hours during a clear day with cirrus. This corresponds to spatial scales of 10 to 50 km.

8) Coefficients of variation of optical depth were found to be less than 1% for a 1 min period of uniform cirrus.

*Acknowledgments*. The authors wish to thank Gary Tannahil and Louis Fowler of the Texas Air Control Board, who operated the instrument and collected data for a dry-front passage over Austin, Tex.

## REFERENCES

Deirmendjian, D., 1964: Scattering and polarization properties of water clouds and hazes in the visible and infrared. *Appl. Opt.*, **3**, 187–196.

Elterman, Louis, 1970: Vertical-attenuation model with eight surface meteorological ranges 2 to 13 kilometers. Environ. Res. Pap. No. 318, Air Force Cambridge Research Laboratories.

Flowers, E. C., R. A. McCormick and K. R. Kurfis, 1969: Atmospheric turbidity over the United States, 1961–1966. *J. Appl. Meteor.*, **8**, 955–962.

Fowle, F. E., 1912: The spectroscopic determination of aqueous vapor. *Astrophys. J.*, **35**, 149–162.

——, 1915: The transparency of aqueous vapor. *Astrophys. J.*, **42**, 394–411.

Gates, David M., 1956: Infrared determination of precipitable water vapor in a vertical column of the earth's atmosphere. *J. Meteor.*, **13**, 369–375.

——, and Walter J. Harrop, 1963: Infrared transmission of the atmosphere to solar radiation. *Appl. Opt.*, **2**, 887–898.

Guzzi, Rodolfo, Claudio Tomasi and Ottavio Vittori, 1972: Evidence of particulate extinction in the near infrared spectrum of the sun. *J. Atmos. Sci.*, **29**, 517–523.

Hansen, J. E., 1969: Exact and approximate solutions for multiple scattering by cloudy and hazy planetary atmospheres. *J. Atmos. Sci.*, **26**, 478–487.

——, 1971: Multiple scattering of polarized light in planetary atmospheres. Part I. The doubling method. *J. Atmos. Sci.*, **28**, 120–125.

Pitts, D. E., William McAllum and Alyce E. Dillinger, 1974a: Measurements of atmospheric precipitable water using a solar radiometer. NASA TM X-58129.

——, T. L. Barnett, C. L. Korb, Walter Hanby and Alyce E. Dillinger, 1974b: Atmospheric transmission computer program CP. NASA TM X-58137.

Shaw, G. E., J. A. Reagan and B. M. Herman, 1973: Investigations of atmospheric extinction using direct solar radiation measurement made with a multiple wavelength radiometer. *J. Appl. Meteor.*, **12**, 374–380.

Sivertsen, Svein, and Jan-Erik Solheim, 1975a: A field instrument for water vapor measurements. *Infrared Phys.*, **15**, 79–82.

——, and ——, 1975b: Atmospheric vapour measurements in Norway from 1972 to 1974. *Infrared Phys.*, **15**, 83–85.

Turner, Robert E., 1975: Atmospheric effects in multispectral remote sensor data. NASA CR-ERIM 109600-15-F.

Volz, F. E., 1969: Some results of turbidity networks. *Tellus*, **21**, 626–629

——, 1974: Economical multispectral sun photometer for measurements of aerosol extinction from 0.44 $\mu$m to 1.6 $\mu$m and precipitable water. *Appl. Opt.*, **13**, 1732–1733.

——, 1975: Volcanic twilights from the Fuego eruption. *Science*, **189**, 48–50.